






Bivalent Transition Metal Complexes of O and N Donor Schiff Base Ligand: Synthesis, Cyclic Voltammetry Studies and Molecular Docking Approach Compatible with Promising Biological Studies

Priyanka R Patil ¹, Rangaswamy Javarappa ², Madalambika ¹, Kumar Ankanashetty pura Chikkachannanjaiah ¹, Nagaraja Naik ^{1,*}

¹ Department of Studies in Chemistry, University of Mysore, Manasagangotri, Mysuru-570006, Karnataka, India; priyankarpatil2021@gmail.com (P.R.P.); maadhuchem@gmail.com (M.); kumar.a.c1994@gmail.com (A.C.K.);

² Department of Chemistry, Poornaprajna College, Shri Admar Mutt Education Council, Mangalore University, Udipi-576101, Karnataka, India.; rangaswamyteertha@gmail.com (J.R.);

* Correspondence: dmaikchem@gmail.com (N.N.);

Scopus Author ID57225381566

Received: 4.10.2022; Accepted: 26.11.2022; Published: 8.02.2023

Abstract: A Schiff base (E)-N'-(4-hydroxy-3,5-dimethoxybenzylidene) nicotinohydrazide (HL) derived from nicotinic acid hydrazide and syringaldehyde was synthesized. Further, HL was treated with respective metal chloride salts of [Mn(II), Co(III), and Ni(II)] to form complexes(1-3). The chemical structure of HL and metal complexes was established employing elemental analysis, UV-Vis, FT-IR, ¹H-NMR, ¹³C-NMR, LC-MS, TGA, and molar conductance data. The electrochemical behavior of the ligand and its complexes were investigated by cyclic voltammetry. The analytical data showed that the metal-to-ligand ratio is 1:2 (M:L). Molar conductivity data showed that all the complexes were non-electrolytic. The octahedral geometry of the complexes was confirmed by UV-visible spectrum and magnetic moment. The IR spectra results show that the ligand is bidentate, coordinating through the azomethine nitrogen and oxygen of the carbonyl group. The molecular docking studies on the P53 cancer mutant protein (PDB ID: 5AB9) were done using the synthesized compounds as potential cancer cell inhibitors. In vitro antioxidant, anticancer and antimicrobial activities for the synthesized ligand and complexes were studied. The observed data infer that all the complexes show promising biological activity against all of the tested free radicals and microbial species compared to the parent ligand.

Keywords: O and N donor Schiff base; cyclic voltammetry; antioxidant; anticancer and molecular docking studies.

© 2023 by the authors. This article is an open-access article distributed under the terms and conditions of the Creative Commons Attribution (CC BY) license (<https://creativecommons.org/licenses/by/4.0/>).

1. Introduction

Treatment that involves high doses of medicines has toxic side effects leading to more complications. So, there is a need to focus on target-specific drugs, thus decreasing side effects [1]. One such promising approach is the use of hydrazone linkers which show the bioavailability of drugs at the diseased site [2]. Hydrazones have an imine group attached to different organic moieties (R), which can be released at the site of infection in a controlled manner. This change in the (R) groups can have various useful applications in diminishing the symptoms or curbing the disease in the first place [3]. Also, aroyl hydrazones of pyridine rings have high sensitivity and selectivity, thus captivating special attention as analytical reagents

[4–9]. Benzimidazoles[10], pyrimidines[11], pyridines[12], and quinazolines[13] also show medicinal properties by forming stable complexes when combined with transition metal ions. Chelation causes sharing of the positive charge of the metal ion with the donor atoms hence veiling its polarity. This increases the lipophilic nature of the metal, thereby amplifying its movement through the lipid layers of the organisms[14,15]. Metals' distinctive characteristics include redox activity[16], coordination modes, and reactivity towards organic moieties. Due to this nature, metals treat various disorders [17].

Transition metals such as manganese, iron, cobalt, nickel, and copper are involved in multiple biological processes where binding to several proteins and enzymes is seen [18]. Transition metals have several oxidation states that make them suitable for interacting with negatively charged molecules. Such properties of transition metals have paved the way for metal-based drugs with large pharmacological applications [19,20]. The use of transition metal complexes as therapeutic agents has become more and more noticeable. These complexes offer a prodigious diversity in their action as anti-inflammatory[21], anti-infective[22], and antidiabetic agents[23]. Significant efforts are made to develop transition metal complexes as drugs[24]. In view of the above importance of Schiff base and its metal complexes, as well as our interest in continuing studies on transition metal complexes [25–27]. Herein, we report the preparation, characterization, and biological applications of a new Schiff base constructed from nicotinic hydrazide and its metal complexes.

2. Materials and Methods

Nicotinic acid hydrazide and syringaldehyde were procured from Sigma Aldrich Chemicals Pvt. Ltd. Bengaluru. The metal salts and solvents were of reagent grade purchased from S.D. fine Chemicals and used without any purification. Elemental analysis was performed using Perkin Elmer 240 CHN analyzer. UV-Vis absorption spectrum was recorded with a JASCO UV spectrophotometer (Model V-730) in the range of 300-800 nm. IR spectra were recorded in the region of 4000–400 cm^{-1} with an FT/IR-4100 type-A spectrometer (KBr disk matrix). NMR spectra (^1H NMR: 400 MHz and ^{13}C NMR: 100 MHz) were recorded on VNMRS-400 Agilent-NMR spectrometer, and chemical shift values (δ) were reported as ppm referenced to tetramethylsilane (TMS). DMSO- d_6 was used as a solvent. Thermal studies were carried out with TGA Q50 V20.10 Build36 in the temperature range 25–1000 $^{\circ}\text{C}$ at a heating rate of 10 $^{\circ}\text{C}$ min^{-1} under a nitrogen atmosphere. Mass spectra were acquired on LC-MS/MS Synapt G2 HDMS. The progress of the reaction was monitored by the use of TLC (silica-coated aluminum plates) under a UV chamber. The molar conductance of the complexes was measured on an Elico CM-180 conductivity meter with a cell having a cell constant of 1 cm^{-1} . Cyclic voltammetry was recorded using a Biologic SP-150 potentiostat. Glassy carbon of 0.196 cm^2 served as the working electrode, while Ag/Ag $^+$ electrode and Pt wire were used as reference and counter electrodes, respectively.

2.1. Chemical synthesis.

2.1.1. Preparation of (E)-N'-(4-hydroxy-3,5-dimethoxybenzylidene)nicotinohydrazide (HL).

To a minimum amount of ethanol, nicotinic hydrazide (1mmol, 0.137g) was added with constant stirring. On complete dissolution, an ethanolic solution of syringaldehyde (1mmol, 0.182g) was added dropwise at around 60 $^{\circ}\text{C}$. The reaction mixture acquired pale yellow color

after 4 hours of reflux. TLC was used to predict the formation of the Schiff base. On cooling, the settled product was filtered, washed with excess ethanol, and re-crystallized with the same.

2.2.2. Synthesis of Mn(II), Co(III) and Ni(II) complexes (1-3).

A stoichiometric amount of metal chlorides of Mn(II), Co(III), and Ni(II) in a minimum amount of hot ethanolic solution was added dropwise to an ethanolic solution of the synthesized ligand HL with metal to ligand ratio of 1:2. The reaction mixture was refluxed at 60°C for 3-4 hours with constant stirring. The change of color was an indication of the complex formation. On cooling, the colored solid obtained was filtered, washed successively with excess ethanol, and dried over a vacuum. The complexes were colored and stable to air and moisture. The complexes were insoluble in most of the polar and non-polar solvents but were soluble in DMSO. An outline of the proposed structures of HL and complexes (1–3) is depicted in Scheme 1 and Figure 1. The melting point, micro-elemental analysis, and m/z data are given in Table 1.

2.2. Biological studies.

2.2.1. Antioxidant activity.

2,2'-Diphenyl-1-picrylhydrazyl (DPPH) radical scavenging assay (RSA). The antioxidant activity of newly synthesized compounds was evaluated by DPPH radical scavenging assay [28]. Internal standard BHA and the synthesized metal complexes (1-3) of different concentrations were prepared in distilled ethanol. 1 mL solution of each compound having different concentrations (10, 25, 50, 100, 200, and 500 µM) was taken in different test tubes along with 4 mL of 0.1M methanolic solution of DPPH and shaken vigorously. The tubes were then incubated in the dark room for 20 min at RT. A DPPH blank was prepared without compound, and ethanol was used for the baseline correction. Changes (decrease) in the absorbance at 517 nm were measured using a UV-visible spectrophotometer, and the remaining DPPH was calculated. The percent decrease in the absorbance was recorded for each concentration, and the percent quenching of DPPH was calculated based on the decrease observed in the absorbance of the radical. The radical scavenging activity was expressed as an inhibition percentage and was calculated using the formula:

$$\text{Radical scavenging activity(\%)} = \frac{A_0 - A_1}{A_1} \times 100$$

where A_0 is the absorbance of the control (blank, without compound) and A_1 is the absorbance of the compound.

Equation 1. Radical scavenging activity formula.

2.2.2. Antimicrobial activity.

HL and its metal complexes (1-3) were screened for their antimicrobial activity using Muller-Hilton (MH) method. The pathogenic bacterial strains (*Escherichia coli*, *Staphylococcus aureus*, and *Bacillus subtilis*) and two fungal strains (*Aspergillus Niger*, *Penicillium rubrum*, and *Candida albicans*) were used [29].

2.2.3. Antibacterial activity.

Briefly, 20 mL of the sterilized agar media was poured into pre-sterilized Petri plates. Excess of the suspension was decanted, and the plates were dried in an incubator at 37 °C for 1 hr. 20 mL of the bacterial suspension (in sterilized MH agar media) was poured into it, swabbed neatly, and allowed to solidify. Wells were made on each Petri plate using a 6 mm sterile cork borer. 100 µL of the test compounds (5mg/mL in DMSO) were added to each of them. The plates were incubated at 37 °C for 24 hrs, and the zone of inhibition (ZI) was measured in millimeters (mm) using a digital micrometer and compared with the reference standard Amoxicillin (5mg/mL). Each experiment was performed in triplicates [30].

2.2.4. Antifungal activity.

Antifungal screening of HL and its metal complexes (1-3) was carried out by a well diffusion method against three fungal strains in sterilized Asthana and Hawker's agar media, as reported earlier [31]. Briefly, the fungal suspension (in 3 mL of saline solution) mixed with 20 mL sterile agar media was poured into Petri plates and solidified. Later, the plates were dried at 37 °C for 1 hr in the incubator. Wells were made using a 6 mm sterile cork borer to which 100 µL of the test compounds (5mg/mL in DMSO) were added. The Petri plates were prepared in triplicates and incubated at 25 °C for 72 hrs. The zone of inhibition (in mm) was measured and compared with the reference fluconazole [32,33].

2.2.5. Anticancer assay.

The inhibition of cell growth by HL and its metal complexes(1-3) were evaluated using 3-(4,5-dimethylthiazol-2-yl)-2,5-diphenyl tetrazolium bromide (MTT) cleavage assay with MCF-7 and HeLa cell lines [34]. The cells were seeded at 1×10^4 cells/well in 96 well plates in RPMI medium supplemented with 10% Fetal Bovine Serum (FBS). After 20 hrs of culture, transition metal complexes and the uncoordinated HL at 10 µM concentration were added in triplicate, and the cells were further cultured for 72 hrs. The cells were then exposed to 5 mg mL^{-1} MTT in Phosphate buffer saline (PBS) at a final concentration of 1 mg mL^{-1} in culture for 5 hrs. Formazan crystals formed during incubation were dissolved overnight at 37°C by adding 10% SDS containing 20mM HCl. The absorbance was measured at 570nm.

2.3. Molecular docking studies.

The Molecular Docking study of ligand HL and the three complexes(1-3) with P53 cancer mutant protein (PDB ID: 5AB9) was performed by using an Autodock tool to know the different interactions between ligand and the protein [35]. The 3-D structure of the P53 cancer mutant protein (PDB ID: 5AB9) was downloaded from the RCSB Protein Data Base in PDB format; the bound ligands were removed using Biovia discovery studio 2019. Using an Autodock tool, polar hydrogen atoms were added, and energy was minimized to the protein[36]. The grid box was generated to define a binding site using a grid size of X=123.62, Y=103.46, and Z=-47.13. The three complexes and ligand molecules were drawn in Marvin JS tool, converted into a 3-D structure, and saved in PDB format. All these compounds were optimized and converted from PDB to PDBQT format by using Autodock tools 4.2.6. The docking analysis has been performed by using the Autodock tool. All the molecules have been docked to the active site of the P53 cancer mutant protein. The binding affinity of the

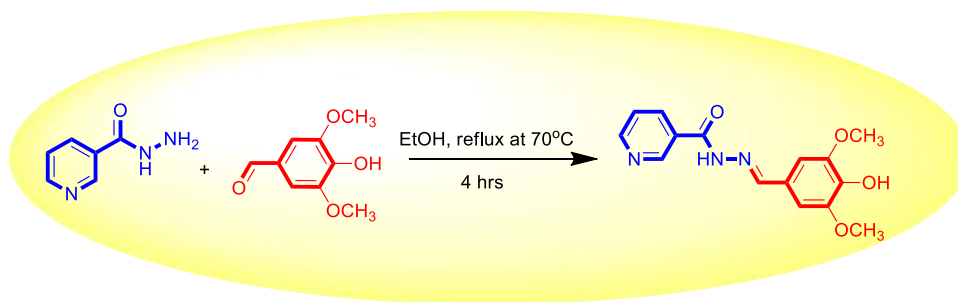
complexes was observed as a negative score with a unit of kcal mol⁻¹. Finally, protein-ligand interactions were analyzed by using the Biovia discovery studio visualizer[37].

3. Results and Discussion

The complexes were generally obtained by refluxing respective transition metal salts with HL at 70°C for 3 hrs in an oil bath with constant stirring. The reaction of HL with MX₂.nH₂O in a (2:1) molar ratio led to the formation of Schiff base metal complexes (1-3).

All the complexes derived from HL were colored, stable, non-hygroscopic, and insoluble in most of the polar and non-polar solvents but were soluble in DMSO. The molar conductivity measurements of all the complexes(1-3) in (1x10⁻³ M) DMSO solution at 25°C are predicted in Table 1. The low molar conductance value (12-18 Ω⁻¹cm² mol⁻¹) indicates their non-electrolytic nature.

The micro-elemental analysis for C, H, N, and M and the molecular weight of the complexes obtained agreed with the predicted formula for the complexes(1-3). An outline of the proposed structures of HL and its complexes (1-3) is depicted in Scheme 1 and Figure 1. The melting point, micro-elemental analysis, and m/z data are given in Table 1.



Scheme 1. Synthesis of ligand HL.

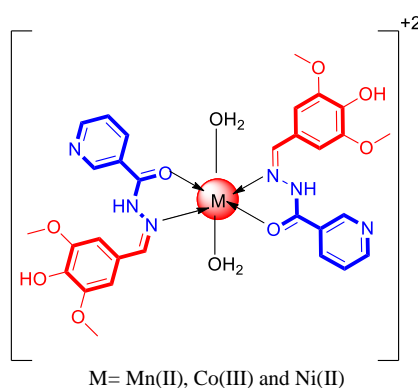


Figure 1. The general structure of the synthesized metal complexes (1-3).

Table 1. Physical parameter of hydrazone Schiff base ligand HL and its metal complexes (1-3).

No.	Empirical Formula	M.W (g/mol)	Color	M.P	Yield (%)	Molar conductance (μs/cm)	C	H	N	M
L	C ₁₅ H ₁₅ N ₃ O ₄ HL	301.11	Cream yellow	214-216	90.2	-	59.73	4.98	13.89	-
1	[Mn(HL) ₂ (H ₂ O) ₂]	693.60	Light yellow	>300	89	15.6	54.75	4.55	12.73	8.31
2	[Co(HL) ₂ (H ₂ O) ₂]	697.53	Dark green	>300	86	12.2	54.43	4.52	12.66	8.86
3	[Ni(HL) ₂ (H ₂ O) ₂]	697.39	yellow	>300	88	18.0	54.46	4.54	12.65	8.82

3.1. IR spectral analysis.

In order to determine the binding mode of ligand to metal in the complexes, the IR spectrum of the ligand was compared to the spectra of metal complexes. The diagnostic IR spectral bands of HL and its metal complexes (1-3) are presented in Table 2 and Figure 2. The band at 1582 cm^{-1} is assigned to the ligand's azomethine ($-\text{C}=\text{N}-$). The IR spectrum of HL additionally showed a broad band at 3222 and 3472 cm^{-1} due to the stretching vibration of ($-\text{NH}$) and ($-\text{OH}$) groups, respectively. On complexation, the bands of the imine group displayed a shift to a higher wave number (1596 , 1592 , and 1588 cm^{-1}) as compared to the free Schiff base ligand (1582 cm^{-1}). Also, the band seen at 1638 cm^{-1} of the carbonyl group of HL was shifted to a higher wave number (1645 , 1648 , and 1659 cm^{-1}) of the three complexes. The shift in the intensities before and after complexation indicates the involvement of these groups in complex formation [38,39]. From the IR spectral data and the results mentioned below, it is concluded that the ligand behaves as a bidentate coordinating through the imine nitrogen and oxygen of the carbonyl group in complexes (1-3). The IR spectrum of all the complexes is predicted in Figure 2.

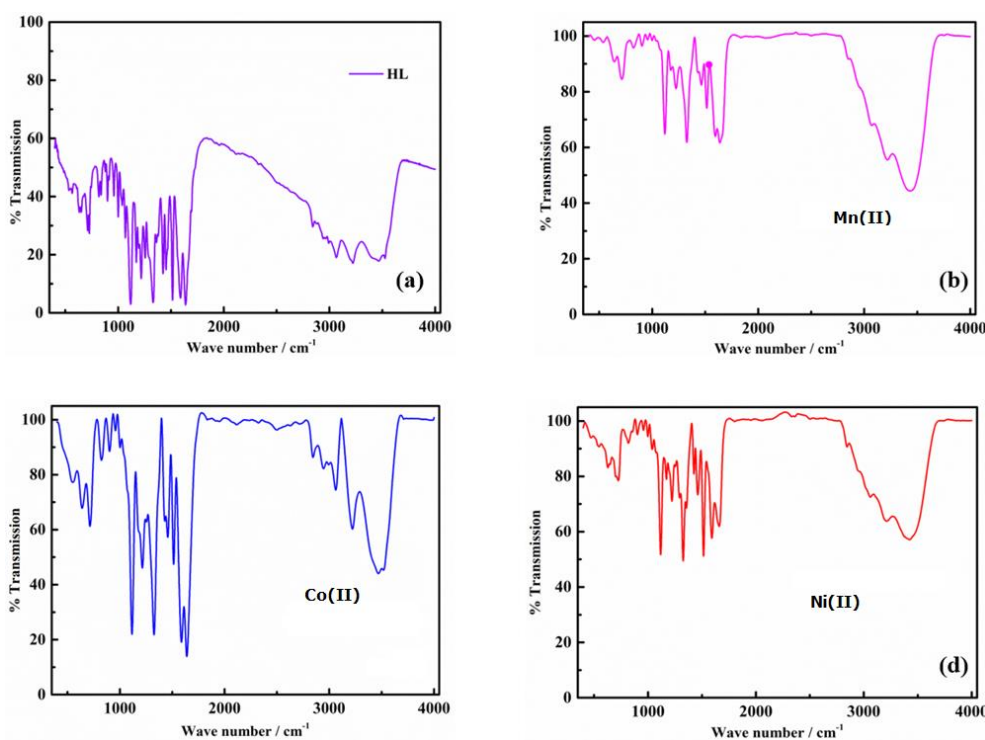


Figure 2. IR spectra of ligand HL and its metal complexes (1-3).

Table 2. IR spectral data of ligand HL and metal complexes (1-3).

L/complexes	$\nu(\text{O-H})$	$\nu(\text{N-H})$	$\nu(\text{C=O})$	$\nu(\text{N-N})$	$\nu(\text{C-O})$	$\nu(\text{C=N})$	$\nu(\text{M-O})$	$\nu(\text{M-N})$
$\text{C}_{15}\text{H}_{15}\text{N}_3\text{O}_4(\text{HL})$	3472	3222	1638	1110	1214	1582	-	-
$[\text{Mn}(\text{HL})_2(\text{H}_2\text{O})_2]$	3436	3215	1645	1123	1223	1596	712	645
$[\text{Co}(\text{HL})_2(\text{H}_2\text{O})_2]$	3433	3195	1648	1120	1235	1592	708	635
$[\text{Ni}(\text{HL})_2(\text{H}_2\text{O})_2]$	3421	3208	1659	1116	1229	1588	718	639

3.2. UV-visible spectra.

The electronic spectral data of ligand HL and its metal complexes were recorded in 10^{-3} M DMF solution in the $300\text{--}800\text{ nm}$ range. In the UV spectrum of ligands, the appearance of two absorption bands at 321 and 410 nm can be assigned to $\pi\text{-}\pi^*$ and $n\text{-}\pi^*$ transitions (Table 3). On the other hand, these transitions in the complexes appeared as bands that were shifted

compared to those of the ligand; specifically, the bands corresponding to $\pi-\pi^*$ and $n-\pi^*$ transitions appeared in the range 325-335 nm and 352-378 nm, respectively. The absorption bands of the Mn(II) complex have been found around 420–526 nm suggesting an octahedral geometry, with the ${}^6A_{1g} \rightarrow {}^4T_{1g}(4G)$, ${}^6A_{1g} \rightarrow {}^4T_{2g}(4G)$ transition for complexes. These bands are reasonably assigned to d–d transition based on their low extinction coefficients[40]. At the same time, the electronic spectrum of the Co(III) complex displayed one band at 490-588 nm attributed to ${}^4T_{1g}(F) \rightarrow {}^4T_{2g}(F)$, ${}^4T_{1g}(F) \rightarrow {}^4A_{2g}(F)$, and ${}^4T_{1g}(F) \rightarrow {}^4T_{2g}(P)$ transitions, respectively, in a high-spin octahedral geometry around the cobalt(III) ion. The electronic spectra of the Ni(II) complex exhibit absorption bands at 512-610 nm, attributable to ${}^3A_{2g} \rightarrow {}^3T_{2g}(F)$, ${}^3A_{2g} \rightarrow {}^3T_{1g}(F)$, and ${}^3A_{2g} \rightarrow {}^3T_{1g}(P)$, transitions, respectively, which indicates octahedral geometry. The UV-visible spectrum and electronic spectral data of ligand and its complexes, along with their absorption band, are depicted in Figure 3 and Table 3.

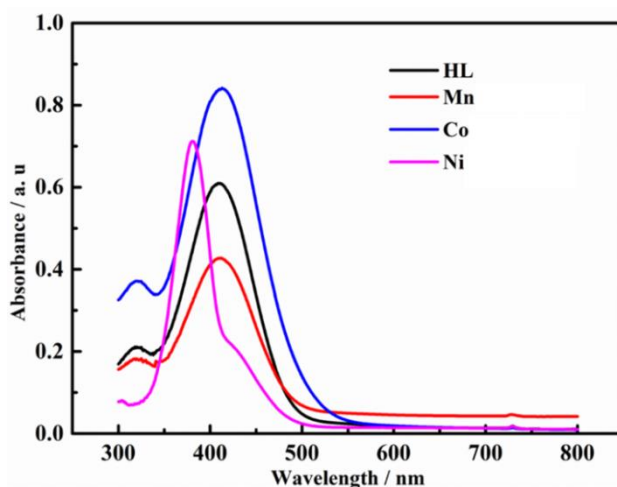


Figure 3. UV-visible spectra of ligand HL and its metal complexes (1-3) in DMSO medium.

Table 3. The UV-visible spectrum and electronic spectral data of ligand and its complexes (1-3).

No.	Complexes	nm	Absorption bands
HL	L	321, 410	$\pi-\pi^*$ and $n-\pi^*$
1	$[Mn(HL)_2(H_2O)_2]$	325, 352 420–526	$\pi-\pi^*$ and $n-\pi^*$ ${}^6A_{1g} \rightarrow {}^4T_{1g}(4G)$, ${}^6A_{1g} \rightarrow {}^4T_{2g}(4G)$
2	$[Co(HL)_2(H_2O)_2]$	332, 365 490-588	$\pi-\pi^*$ and $n-\pi^*$ ${}^4T_{1g}(F) \rightarrow {}^4T_{2g}(F)$, ${}^4T_{1g}(F) \rightarrow {}^4A_{2g}(F)$ and ${}^4T_{1g}(F) \rightarrow {}^4T_{2g}(P)$
3	$[Ni(HL)_2(H_2O)_2]$	335, 378 512-610	$\pi-\pi^*$ and $n-\pi^*$ ${}^3A_{2g} \rightarrow {}^3T_{2g}(F)$, ${}^3A_{2g} \rightarrow {}^3T_{1g}(F)$ and ${}^3A_{2g} \rightarrow {}^3T_{1g}(P)$,

3.3. 1H and ${}^{13}C$ NMR spectroscopy.

1H and ${}^{13}C$ NMR spectroscopy of HL was recorded in DMSO- d_6 and are given in Figures S1 and S2. The hydrogen of the azomethine ($-CH=N$)- group shows a singlet peak at 8.29 ppm. The multiplet signals of aromatic-hydrogen were observed between 6.96-9.01 ppm. The di-methoxy ($-OCH_3$) protons resonate at 3.78 ppm. The structure of the ligand HL was evaluated further using ${}^{13}C$ NMR. The signal at $\delta=148.24$ ppm is attributed to the carbon of the azomethine group ($-CH=N$). The peaks observed between $\delta=104.6-148.78$ ppm show the aromatic ring carbons. The peak at 161.63 ppm corresponds to the carbon of the amide group. The spectrum is shown in Figures S1 and S2.

3.4. Mass spectrometry.

Molecular ion peaks of the ligand HL and its complexes (1-3) were observed at different intensities in positive ionization mode, which confirmed the molecular weights. The mass spectrum of HL and its complexes are depicted in Figures S3-S6. The M+1 peak observed at $m/z=302.10$ is consistent with the molecular mass of the ligand. The mass spectrum shows molecular ion peaks at $m/z= 693.60, 697.53,$ and $697.39,$ which confirms the mass of the synthesized metal complexes (1-3), respectively.

3.5. Thermogravimetric analysis.

The TGA thermo analytical curves of $[\text{Mn}(\text{HL})_2(\text{H}_2\text{O})_2]$ show mass loss (Calc./Found%: 14.45/5.20) with DTG peak at 45°C , assigned to the loss of two coordinated water molecules within the temperature range of $95\text{--}290^\circ\text{C}$. The thermo analytical curves showed the second step of decomposition within the temperature range $290\text{--}340^\circ\text{C}$ with mass loss of (Calc./Found%:40.35/41.35) associated with DTG peaks at 290°C leaving off the organic moiety, i.e., the ligand. In the last step, MnO, the metal oxide (Calc./Found%: 63.65/62.50), remains as the final residue. The decomposition step of $[\text{Co}(\text{HL})_2(\text{H}_2\text{O})_2]$ complex started with the breaking of the H-bond of water molecule associated with an endothermic peak at 46°C , followed by the loss of two water molecules with an endothermic peak at $77\text{--}130^\circ\text{C}$ showing 5.20% weight loss (Calc. 5.35%). A DTA peak was observed at 246°C and 312°C with 52.10% weight loss (Calc. 52.05%). It can be owed to the loss of two organic ligands. Oxidative thermal decomposition occurred in the $365\text{--}650^\circ\text{C}$ temperature range with an exothermic peak leaving CoO with 82.50% weight loss (Calc. 82.70%). The first decomposition step for complex (3) began with the elimination of two water molecules at $76\text{--}185^\circ\text{C}$ with a weight loss of about 11.25% (Calc. 11.05%). Another thermal decomposition peak at $215\text{--}410^\circ\text{C}$ shows a weight loss of approximately 59.45 % (Calc.59.56%) due to a coordinated organic moiety loss. Finally, the complex showed exothermic peaks in the temperature range of $435, 455^\circ\text{C}$ corresponding to oxidative thermal decomposition, which proceeded gradually with a final residue of NiO at $455\text{--}790^\circ\text{C}$. TGA and DTA curves of complexes (1-3) are depicted in Figure 4.

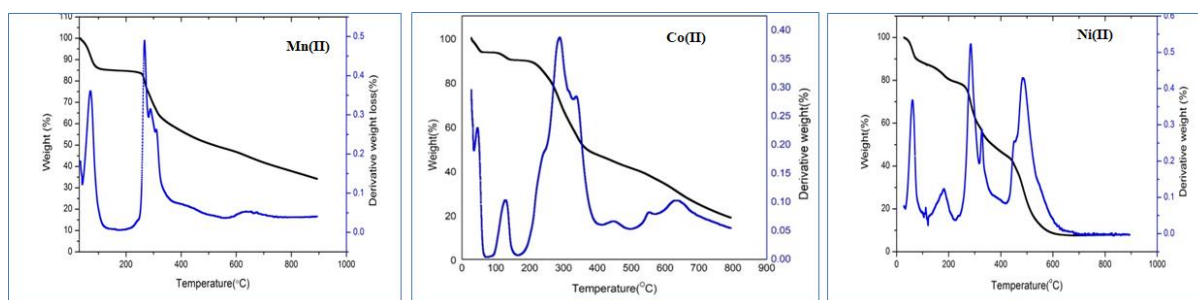


Figure 4. TGA and DTA curves of complexes (1-3).

3.6. Cyclic voltammetry.

Cyclic voltammetry of the ligand HL and its complexes(1-3) is compared against a blank electrolyte (0.1 M TBAPF₆ in DMSO) to understand the redox behavior of the complexes. The reduction peak at $-1.3\text{ V vs. Ag/Ag}^+$ in the blank is for the trace amount of oxygen present in the medium. In the case of ligands and complexes, the same redox peak is shifted to negative potential indicating the increase in overpotential for the oxygen reduction

reaction upon the incorporation of ligands and complexes. HL shows redox behavior in the potential window of 0.0 to 0.8 V, which is also observed in all the complexes, indicating the presence of ligands in the complexes. This redox behavior of the ligand could be due to the presence of secondary amines and pyridinic nitrogen [41]. Redox species containing N center are known to show redox activity in this redox potential. However, only $[\text{Mn}(\text{HL})_2(\text{H}_2\text{O})_2]$ and $[\text{Ni}(\text{HL})_2(\text{H}_2\text{O})_2]$ show an additional reversible redox peak around -1.6 V vs. Ag/Ag^+ . This could be due to the redox behavior of metal centers in respective complexes. However, this peak is not observed in the case of $[\text{Co}(\text{HL})_2(\text{H}_2\text{O})_2]$, indicating metal center may not show redox activity in the complex.

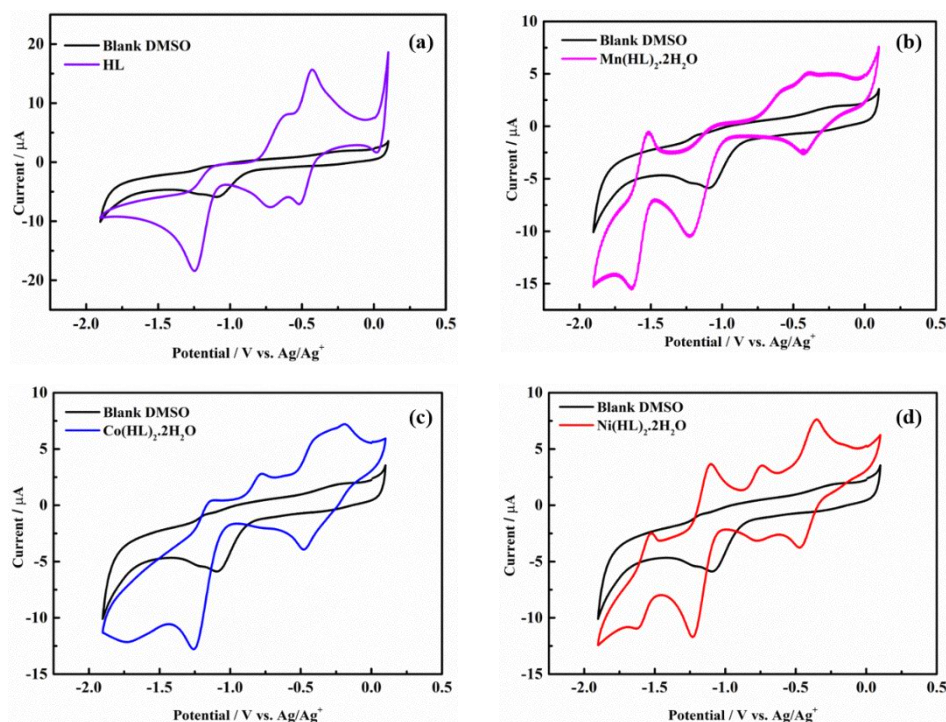


Figure 5. CV of (a) HL ligand, (b) $[\text{Mn}(\text{HL})_2(\text{H}_2\text{O})_2]$, (c) $[\text{Co}(\text{HL})_2(\text{H}_2\text{O})_2]$ and (d) $[\text{Ni}(\text{HL})_2(\text{H}_2\text{O})_2]$ compared with blank DMSO medium.

3.7. Biological evaluation.

3.7.1. Antioxidant activity.

The radical scavenging activity of ligand HL and the complexes (1-3) was done by using *in vitro* assay of 2,2-diphenyl-1-picryl-hydrazyl (DPPH). The antioxidant properties were expressed as 50 % inhibitory concentration (IC_{50}) values. DPPH is one of the simplest and best methods to detect the radical scavenging activity of natural extracts or synthesized compounds due to its stability as a free radical with an odd electron. Therefore, the free radical scavenging capacity of HL and its complexes have been evaluated using this method against BHA as a positive standard. Initially, HL exhibited a certain amount of antioxidant efficacy, which may be due to the presence of an electron-donating dimethoxy group and hydroxyl group on the phenyl ring of aldehyde. Upon complexation with their respective metal ions, $[\text{Mn}(\text{II})]$, $[\text{Co}(\text{III})]$, and $[\text{Ni}(\text{II})]$, we observed an increase in their antioxidant potency. Among the synthesized complexes $[\text{Co}(\text{HL})_2(\text{H}_2\text{O})_2]$ and $[\text{Ni}(\text{HL})_2(\text{H}_2\text{O})_2]$ showed the highest antioxidant activity leading to a lower IC_{50} value. The inhibitory effects of HL and its complexes (1-3) are shown in Figure 6 and Table 4.

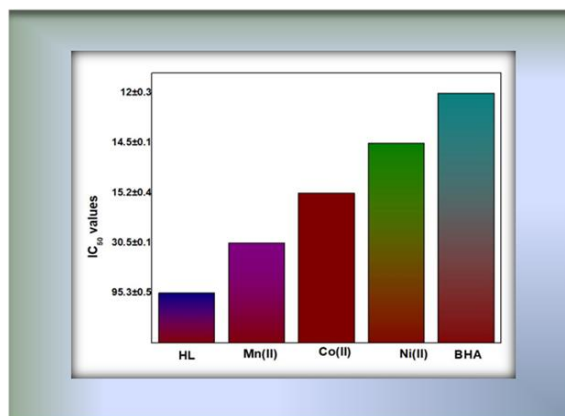


Figure 6. IC₅₀ inhibitory concentration of ligand HL and its complexes(1-3) for 50% of DPPH radical.

Table 4. 50% inhibitory concentration (IC₅₀)Radical scavenging activity of ligand HL and metal complexes (1-3).

Sl. No.	Compound	IC ₅₀
1	HL	95.3±0.5
2	[Mn(HL) ₂ (H ₂ O) ₂]	30.5±0.1
3	[Co(HL) ₂ (H ₂ O) ₂]	15.2±0.4
4	[Ni(HL) ₂ (H ₂ O) ₂]	14.5±0.1
5	BHA	12±0.3

3.7.2. Antimicrobial activity.

The antimicrobial activity of HL and its derived metal complexes(1-3) were evaluated by using the Muller-Hilton (MH) method, in which the inhibitory activity was calculated as the diameter of the inhibition zone (in mm). In the presence of HL and its derived metal complexes, the growth of bacterial and fungal species was pointedly inhibited without any interruption of other external agents. Among the tested complexes [Mn(HL)₂(H₂O)₂]and [Ni(HL)₂(H₂O)₂]showed the highest microbial inhibition effect against the tested bacterial (*B. Subtilis* and *E. Coli*) and fungal (*P. Rubrum*) strains. This may be because manganese is an essential trace nutrient in living cell life and a wide group of enzymes has manganese as a cofactor[42]. From the experimental observations, the antimicrobial activity against all the microbes can be put in the order of HY<Co(III)<Ni(II)<Mn(II)<Amoxicillin/ Fluconazole. Figure 7 and Table 5 show the antimicrobial activity of HL and its complexes compared to amoxicillin/ Fluconazole.

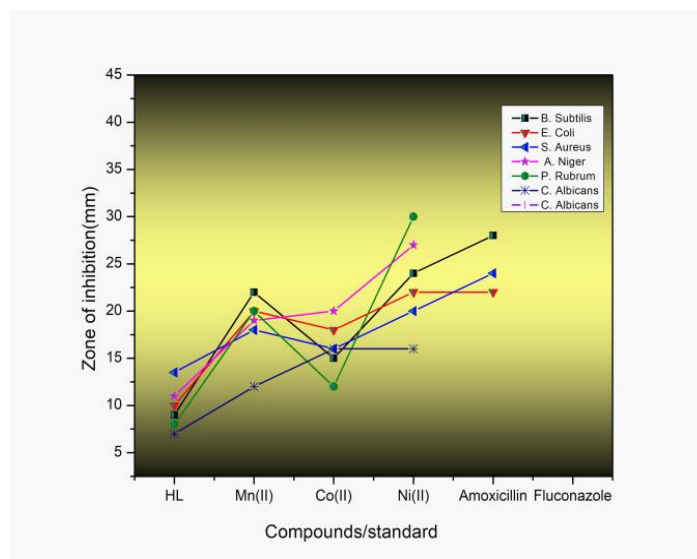


Figure 7. Graphical representation of the antimicrobial activity of HL and its complexes(1-3).

Table 5 Antimicrobial activity of HL and its complexes (1-3).

Sl. No.	Metal complexes	Zone of inhibition (mm)					
		Bacteria			Fungi		
		<i>B. Subtilis</i>	<i>E. Coli</i>	<i>S. Aureus</i>	<i>A. Niger</i>	<i>P. Rubrum</i>	<i>C. Albicans</i>
1	HL	09	10	13.5	11	08	07
2	[Mn(HL) ₂ (H ₂ O) ₂]	22	20	18	19	20	12
3	[Co(HL) ₂ (H ₂ O) ₂]	15	18	16	20	12	16
4	[Ni(HL) ₂ (H ₂ O) ₂]	24	22	20	27	30	16
5	Amoxicillin	28	22	24	NT	NT	NT
6	Fluconazole	NT	NT	NT	31	40	35

3.7.3. Anticancer activity.

The anticancer activity of HL and its complexes(1-3) were studied against MCF-7 breast cell line and HeLa cell lines. The activity included the measurement of % *in vitro* cell inhibition by using MTT colorimetric assay at two different concentrations, 10 μM, and 25 μM. The anticancer activity of the synthesized Schiff base ligand HL and its metal complexes (1-3) are shown in Table 6. Initially, HL exhibits a certain degree of activity due to electron-donating methoxy and a hydroxy group. Upon complexation with Mn(II), Co(III), and Ni(II) metal ions, enhancement in activity was observed. The percentage of activity indicates that complexes (2 and 3) have excellent inhibitory activity against MCF-7 as well as HeLa cancer cells at 25μM. The [Mn(HL)₂(H₂O)₂] complex can make cancer cells undergo apoptosis *in vitro* in a concentration-dependent way, which can inhibit the proliferation of MCF-7 cancer cells[43]. Thus, the [Mn(HL)₂(H₂O)₂] complex could be a potential cancer drug. In contrast, Ni(II) complexes showed moderate activity compared to the Mn(II) complex but higher than that of the ligand HL [44]. Furthermore, molecular docking analysis was performed with cancer mutant protein, and the binding energy of Mn(II) and Co(III) complexes were checked, which proved to be extremely favorable (-8.53 and -6.83kcal/mol)

Table 6. (%) Anticancer activity of HL and its metal complexes.

Sl.No	Compounds	Percentage of Activity			
		MCF-7		HeLa	
		10 μM	25μM	10 μM	25 μM
1	HL	50.60	70.80	40.30	73.55
2	[Mn(HL) ₂ (H ₂ O) ₂]	70.65	90.35	65.30	92.15
3	[Co(HL) ₂ (H ₂ O) ₂]	55.30	75.60	50.40	75.35
4	[Ni(HL) ₂ (H ₂ O) ₂]	53.16	72.25	49.36	74.12
5	Cisplatin	75.45	96.10	70.45	97.35

3.7.4.Molecular docking studies.

The docking analysis of complex compounds (1-3) with P53 cancer mutant protein (5AB9)was analyzed. All the complex compounds and ligand molecule HL were found to exhibit a good interaction with the P53 cancer mutant protein (PDB ID: 5AB9), and their interaction with the binding site of 5AB9 was displayed in Figures 8-11. Among these three complexes, Mn(II) and Co(III) complexes exhibited the best possible interaction with P53 cancer mutant protein (5AB9) residues of CYS220, PRO151, PRO153, THR150, PRO222, and GLU221 with binding energy -8.53and -6.83kcal/mol which includes interactions such as hydrogen bonding, alkyl, π-alkyl, and π-anion are suggesting a high affinity for the binding pocket. The Ni(II) complex showed binding energy of -5.32kcal/mol with the P53 cancer mutant protein. The binding modes of the compounds are in the active binding pocket. Whereas

the ligand HL binds protein (PDB ID:5AB9) residues of LEU145, VAL147, PRO223, CYS220, PRO222, and PRO153 with various interactions like hydrogen bonding, alkyl, and π -alkyl with a binding energy of -5.13 kcal/mol. The detailed interactions have been shown in Figures 8-11, and docking energies are given in Table 6. Thus, it indicates that Mn(II) and Co(III) complexes favor the P53 cancer mutant protein over Ni(II) complex.

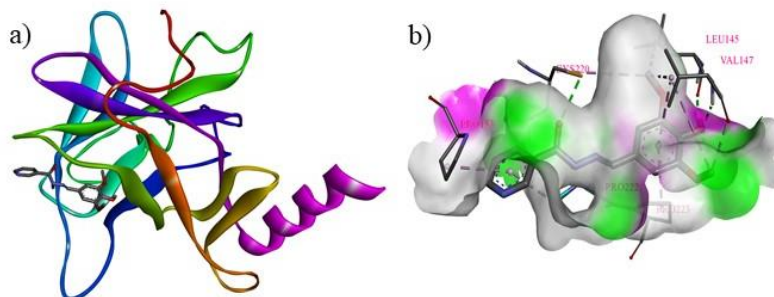


Figure 8. Molecular docking of ligand HL with P53 cancer mutant protein (a) 3-D P53 cancer mutant protein - HL interaction and (b) active site amino acid residues interactions with ligand HL.

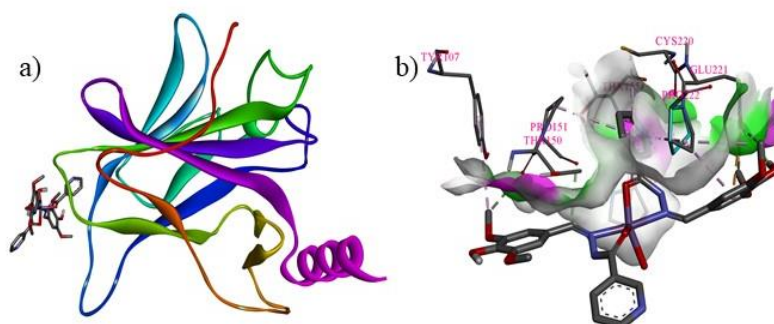


Figure 9. Molecular docking of Mn(II) complex with P53 cancer mutant protein (a) 3-D P53 cancer mutant protein-Mn(II) complex interaction and (b) active site amino acid residues interactions with Mn(II) complex.

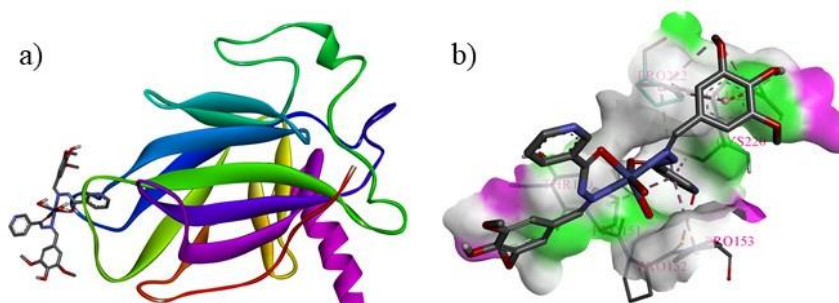


Figure 10. Molecular docking of Co(III) complex with P53 cancer mutant protein (a) 3-D P53 cancer mutant protein-Co(III) complex interaction and (b) active site amino acid residues interactions with Co(II) complex.

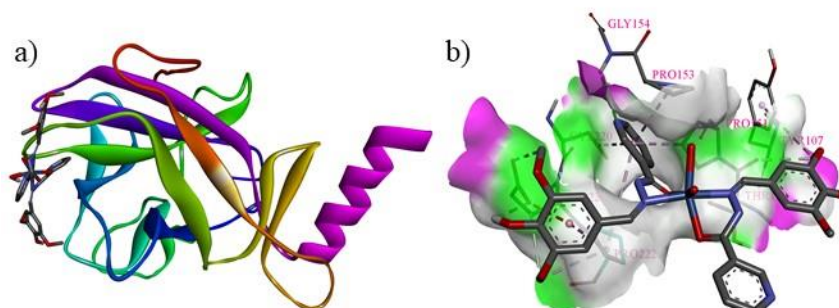


Figure 11. Molecular docking of Ni(II) complex with P53 cancer mutant protein (a) 3-D P53 cancer mutant protein-Ni(II) complex interaction and (b) active site amino acid residues interaction with Ni(II) complex.

Table 6. Docking score of ligand HL and complexes(1-3).

Compound	5AB9 Binding energy (kcal/mol)
HL	-5.13
[Mn(HL) ₂ (H ₂ O) ₂]	-8.53
[Co(HL) ₂ (H ₂ O) ₂]	-6.83
[Ni(HL) ₂ (H ₂ O) ₂]	-5.32

4. Conclusions

In the present study, new class of Mn(II), Co(III) and Ni(II) complexes of azo-containing schiff base of the type [Mn(HL)₂(H₂O)₂],[Co(HL)₂(H₂O)₂] and [Ni(HL)₂(H₂O)₂] where, HL= (E)-N'-(4-hydroxy-3,5-dimethoxybenzylidene)nicotinohydrazide metal was synthesised and characterized by physico-chemical methods. Elemental analyses reveal that the complexes have a ligand-to-metal ratio (2:1). The molar conductance data showed that the complexes are non-electrolytic. Electronic absorption studies demonstrate the ligand coordinates through azomethine nitrogen and oxygen atoms from the carbonyl group reveal the octahedral geometry of the synthesized complexes. ¹H-NMR, ¹³C-NMR, and ESI-MS data support the structure of HL and the complexes. IR spectral data reveals the bidentate nature of the ligand. From the cyclic voltammetry experiment, it is seen that Mn(II) and Ni(II) show an additional reversible redox peak around -1.6 V vs. Ag/Ag⁺. This could be due to the redox behavior of metal centers in respective complexes. TGA gave a clear idea of the degradation and stability of the complexes formed. The presence of an azo moiety and the free methoxy and hydroxy groups in the ligand enhanced the antioxidant activity of complexes. The antibacterial and antifungal data presented in this paper allow us to state that the Mn(II) and Ni(II) complexes show the highest antimicrobial activity compared to the ligand but less than the standards. Mn(II) complex showed the highest anticancer activity compared to the ligand HL, Co(III) and Ni(II) complexes. A molecular docking study indicates that Mn(II) complex favors the P53 cancer mutant protein over other complexes.

Funding

This research received no external funding

Acknowledgments

The authors are thankful to the Institute of Excellence, Vijnana Bhavana, University of Mysore, Manasagangotri, Mysuru, for providing us with spectral data.

Conflicts of Interest

The authors declare no conflict of interest.

References

1. Gashaw, I.; Ellinghaus, P.; Sommer, A.; Asadullah, K. What makes a good drug target? *Drug Discovery Today* **2011**, *16*, 1037–1043, <https://doi.org/10.1016/j.drudis.2011.09.007>.
2. Greenfield, R.S.; Kaneko, T.; Daus, A.; Edson, M.A.; Fitzgerald, K.A.; Olech, L.J.; Grattan, J.A.; Spitalny, G.L.; Braslawsky, G.R. Evaluation in vitro of adriamycin immunoconjugates synthesized using an acid-sensitive hydrazone linker. *Cancer Research* **1990**, *50*, 6600–6607, PMID:2208122.
3. Kölmel, D.K. Kool, E.T. Oximes and hydrazones in bioconjugation: mechanism and catalysis. *Chemical Reviews* **2017**, *117*, 10358–10376, <https://doi.org/10.1021/acs.chemrev.7b00090>.

4. Galić, N.; Perić, B.; Kojić-Prodić, B.; Cimerman, Z. Structural and spectroscopic characteristics of aroylhydrazones derived from nicotinic acid hydrazide. *Journal of Molecular Structures* **2001**, *559*, 187–194, [https://doi.org/10.1016/S0022-2860\(00\)00703-1](https://doi.org/10.1016/S0022-2860(00)00703-1).
5. Gallego, M.; Valcarcel, M.; Garcia-Vargas, M. Spectrofluorimetric and spectrophotometric determination of aluminium with the salicyloylhydrazones of pyridine-2-aldehyde and pyridoxal. *Analyst* **1983**, *108*, 92–98, <https://doi.org/10.1039/AN9830800092>.
6. Manuel-Vez, M.P.; Garcia-Vargas, M. Fluorimetric determination traces of aluminium in soil extracts. *Talanta* **1994**, *41*, 1553–1559, [https://doi.org/10.1016/0039-9140\(94\)E0072-Y](https://doi.org/10.1016/0039-9140(94)E0072-Y).
7. Bale, M.N.; Dave, D.P.; Sawant, A.D. Extraction and spectrophotometric determination of lead (II) with pyridine-2-acetaldehydesalicyloylhydrazone. *Talanta* **1995**, *42*, 129–1296, [https://doi.org/10.1016/0039-9140\(95\)01578-Y](https://doi.org/10.1016/0039-9140(95)01578-Y).
8. Cimerman, Z.; Miljanić, S.; Galić, N. Schiff bases derived from aminopyridines as spectrofluorimetric analytical reagents. *Croatica Chemica Acta* **2000**, *73*, 81–95, <https://hrcak.srce.hr/132084>.
9. Babaiah, O.; Rao, C.K.; Reddy, T.S.; Reddy, V.K. Rapid, selective, direct and derivative spectrophotometric determination of titanium with 2, 4-dihydroxybenzaldehyde isonicotinoyl hydrazone. *Talanta* **1996**, *43*, 551–558, [https://doi.org/10.1016/0039-9140\(95\)01766-6](https://doi.org/10.1016/0039-9140(95)01766-6).
10. El-Sayed, Y.S.; Gaber, M.; El-Nahass, M.N. Structural elucidation, spectroscopic, and metalochromic studies of 2-(2-hydroxy phenyl)-1-H-benzimidazole complexes: Metal ions sensing, DNA binding, and antimicrobial activity evaluation. *Journal of Molecular Structure* **2021**, *1229*, 129809, <https://doi.org/10.1016/j.molstruc.2020.129809>.
11. Saleem, S.H.S.; Sankarganesh, M.; Raja, J.D.; Jose, P.R.A.; Sakthivel, A.; Jeyakumar, T.C.; Asha, R.N. Synthesis, characterization, DFT calculation, biological and molecular docking of Cu (II) complex of pyrimidine derived Schiff base ligand. *Journal of Saudi Chemical Society* **2021**, *25*, 101225, <https://doi.org/10.1016/j.jscs.2021.101225>.
12. Kutlu, E.; Emen, F.M.; Kismali, G.; Kınaytürk, N.K.; Kılıç, D.; Karacolak, A.I.; Demirdögen, R.E. Pyridine derivative platinum complexes: Synthesis, molecular structure, DFT and initial anticancer activity studies. *Journal of Molecular Structure* **2021**, *1234*, 130191, <https://doi.org/10.1016/j.molstruc.2021.130191>.
13. Ghanghas, P.; Choudhary, A.; Kumar, D.; Poonia, K. Coordination metal complexes with Schiff bases: Useful pharmacophores with comprehensive biological applications. *Inorganic Chemistry Communications* **2021**, *130*, 108710, <https://doi.org/10.1016/j.inoche.2021.108710>.
14. Kontoghiorghes, G.J.; Kolnagou, A.; Demetriou, T.; Neocleous, M.; Kontoghiorghes, C.N. New era in the treatment of iron deficiency anaemia using trimaltol iron and other lipophilic iron chelator complexes: historical perspectives of discovery and future applications. *International Journal of Molecular Sciences* **2021**, *22*, 5546, <https://doi.org/10.3390/ijms22115546>.
15. Mandel, S.; Amit, T.; Bar-Am, O.; Youdim, M.B.H. Iron dysregulation in Alzheimer's disease: multimodal brain permeable iron chelating drugs, possessing neuroprotective-neurorescue and amyloid precursor protein-processing regulatory activities as therapeutic agents. *Progress in Neurobiology* **2007**, *82*, 348–360, <https://doi.org/10.1016/j.pneurobio.2007.06.001>.
16. Li, B.; Geoghegan, B.L.; Wolper, C.; Cutsail III, G.E.; Schulz, S. Redox Activity of Noninnocent 2, 2'-Bipyridine in Zinc Complexes: An Experimental and Theoretical Study. *ACS omega* **2021**, *6*, 18325–18332, <https://doi.org/10.1021/acsomega.1c02201>.
17. Das, N.; Raymick, J.; Sarkar, S. Role of metals in Alzheimer's disease. *Metabolic Brain Disease* **2021**, *36*, 1627–1639, <https://doi.org/10.1007/s11011-021-00765-w>.
18. Antelo, G.T.; Vila, A.J.; Giedroc, D.P.; Capdevila, D.A. Molecular evolution of transition metal bioavailability at the host–pathogen interface. *Trends in Microbiology* **2021**, *29*, 441–457, <https://doi.org/10.1016/j.tim.2020.08.001>.
19. Chaudhary, N.K.; Guragain, B.; Chaudhary, S.K.; Mishra, P. Schiff base metal complex as a potential therapeutic drug in medical science: A critical review. *Bibechana* **2021**, *18*, 214–230, <https://doi.org/10.3126/bibechana.v18i1.29841>.
20. Yaşar, Ü.; Gönül, İ.; Türkeş, C.; Demir, Y.; Beydemir, S. Transition metal complexes of bidentate Schiff Base ligands: In vitro and silico evaluation as non classical carbonic anhydrase and potential acetylcholinesterase inhibitors. *ChemistrySelect* **2021**, *6*, 7278–7284, <https://doi.org/10.1002/slct.202102082>.
21. García-Valdivia, A.A.; Jannus, F.; García-García, A.; Choquesillo-Lazarte, D.; Fernández, B.; Medina-O'donnell, M.; Lupiáñez, J.A.; Cepeda, J.; Reyes-Zurita, F.J.; Rodríguez-Diéguez, A. Anticancer and anti-

- inflammatory activities of a new family of coordination compounds based on divalent transition metal ions and indazole-3-carboxylic acid. *Journal of inorganic Biochemistry* **2021**, *215*, 111308, <https://doi.org/10.1016/j.jinorgbio.2020.111308>.
22. Ferreira, M.; Gameiro, P. Fluoroquinolone-transition metal complexes: A strategy to overcome bacterial resistance. *Microorganisms* **2021**, *9*, 1506, <https://doi.org/10.3390/microorganisms9071506>.
 23. El-Megharbel, S.M.; Al-Baqami, N.M.; Al-Thubaiti, E.H.; Qahl, S.H.; Albogami, B.; Hamza, R.Z. Antidiabetic Drug Sitagliptin with Divalent Transition Metals Manganese and Cobalt: Synthesis, Structure, Characterization Antibacterial and Antioxidative Effects in Liver Tissues. *Current Issues in Molecular Biology* **2022**, *44*, 1810–1827, <https://doi.org/10.3390/cimb44050124>.
 24. Silva, M.J.S.A.; Gois, P.M.P.; Gasser, G. Unveiling the Potential of Transition Metal Complexes for Medicine: Translational in Situ Activation of Metal Based Drugs from Bench to in Vivo Applications. *ChemBioChem* **2021**, *22*, 1740–1742, <https://doi.org/10.1002/cbic.202100015>.
 25. Nellufar.; Rangaswamy, J.; Ankali, K.N.; Naik, N.; Nuthan, B.R.; Satish, S. The Mn (II), Co (II), Ni (II) and Cu (II) complexes of (Z)-N' ((1H-indol-3-yl) methylene) nicotinohydrazide Schiff base: synthesis, characterization and biological evaluation. *Journal of Iranian Chemical Society* **2022**, 1–12, <https://doi.org/10.1007/s13738-022-02580-1>.
 26. Revanna, B.N.; Madegowda, M.; Rangaswamy, J.; Naik, N. A novel Schiff base derivative as a fluorescent probe for selective detection of Cu²⁺ ions in buffered solution at pH 7.5: Experimental and quantum chemical calculations. *Journal Molecular Structure* **2022**, *1254*, 132327, <https://doi.org/10.1016/j.molstruc.2021.132327>.
 27. Sekhar, E.V.; Rangaswamy, J.; Bhat, M.; Naik, N. 2-(4-nitrophenyl) iminomethyl phenol Schiff base metal complexes: Synthesis, spectroscopic characterization, anticancer and antimicrobial studies. *Inorganic and Nano-Metal Chemistry* **2022**, 1–10, <https://doi.org/10.1080/24701556.2022.2048019>.
 28. Blois, M.S. Antioxidant determinations by the use of a stable free radical. *Nature* **1958**, *181*, 1199–1200, <https://doi.org/10.1038/1811199a0>.
 29. Balouiri, M.; Sadiki, M.; Ibsouda, S.K. Methods for in vitro evaluating antimicrobial activity: A review. *Journal of Pharmaceutical Analysis* **2016**, *6*, 71–79, <https://doi.org/10.1016/j.jpha.2015.11.005>.
 30. Al-Resayes, S.I.; Shakir, M.; Shahid, N.; Azam, M.; Khan, A.U. Synthesis, spectroscopic characterization and in vitro antimicrobial studies of Schiff base ligand, H2L derived from glyoxalic acid and 1,8-diaminonaphthalene and its Co(II), Ni(II), Cu(II) and Zn(II) complexes. *Arabian Journal of Chemistry* **2016**, *9*, 335–343, <https://doi.org/10.1016/j.arabjc.2011.11.004>.
 31. Sheikh, R.A.; Wani, M.Y.; Shreaz, S.; Hashmi, A.A. Synthesis, characterization and biological screening of some Schiff base macrocyclic ligand based transition metal complexes as antifungal agents. *Arabian Journal of Chemistry* **2016**, *9*, S743–S751, <https://doi.org/10.1016/j.arabjc.2011.08.003>.
 32. Younis, A.M.; Rakha, T.H.; El-Gamil, M.M.; El-Reash, G.M.A. Spectroscopic and theoretical studies on some carbohydrazone complexes and evaluation of their biological potency, catalytic, and ionophore activities. *Journal of Molecular Structure* **2021**, *1245*, 131110, <https://doi.org/10.1016/j.molstruc.2021.131110>.
 33. Saranya, J.; Jone Kirubavathy, S.; Chitra, S.; Zarrouk, A.; Kalpana, K.; Lavanya, K.; Ravikiran, B. Tetradentate Schiff Base complexes of transition metals for antimicrobial activity. *Arabian Journal for Science and Engineering* **2020**, *45*, 4683–4695, <https://doi.org/10.1007/s13369-020-04416-7>.
 34. Mosmann, T. Rapid colorimetric assay for cellular growth and survival: application to proliferation and cytotoxicity assays. *Journal of Immunological Methods* **1983**, *65*, 55–63, [https://doi.org/10.1016/0022-1759\(83\)90303-4](https://doi.org/10.1016/0022-1759(83)90303-4).
 35. Diab, M.A.; Mohamed, G.G.; Mahmoud, W.H.; El-Sonbati, A.Z.; Morgan, S.M.; Abbas, S.Y. Inner metal complexes of tetradentate Schiff base: Synthesis, characterization, biological activity and molecular docking studies. *Applied Organometallic Chemistry* **2019**, *33*, e4945, <https://doi.org/10.1002/aoc.4945>.
 36. Konakanchi, R.; Mallela, R.; Guda, R.; Kotha, L.R. Synthesis, characterization, biological screening and molecular docking studies of 2-aminonicotinaldehyde (ANA) and its metal complexes. *Research on Chemical Intermediates* **2018**, *44*, 27–53, <https://doi.org/10.1007/s11164-017-3089-y>.
 37. Mahesha.; Hema, M.K.; Karthik, C.S.; Pampa, K.J.; Mallu, P.; Lokanath, N.K. Solvent induced mononuclear and dinuclear mixed ligand Cu (II) complex: structural diversity, supramolecular packing polymorphism and molecular docking studies. *New Journal of Chemistry* **2020**, *44*, 18048–18068, <https://doi.org/10.1039/D0NJ03567J>.
 38. Anitha, C.; Sumathi, S.; Tharmaraj, P.; Sheela, C.D. Synthesis, characterization, and biological activity of some transition metal complexes derived from novel hydrazone azo schiff base ligand. *International Journal*

- of Inorganic Chemistry* **2011**, *2011*, 493942, <https://doi.org/10.1155/2011/493942>.
39. Bhaskar, R.S.; Ladole, C.A.; Salunkhe, N.G.; Barabde, J.M.; Aswar, A.S. Synthesis, characterization and antimicrobial studies of novel ONO donor hydrazone Schiff base complexes with some divalent metal(II)ions. *ArabianJournalofChemistry* **2020**, *13*, 6559-6567, <https://doi.org/10.1016/j.arabjc.2020.06.012>.
 40. Raman, N.; Jeyamurugan, R.; Sakthivel, A.; Mitu, L. Novel metal-based pharmacologically dynamic agents of transition metal (II) complexes: designing, synthesis, structural elucidation, DNA binding and photo-induced DNA cleavage activity. *Spectrochimica Acta Part A: Molecular and Biomolecular Spectroscopy* **2010**, *75*, 88–97, <https://doi.org/10.1016/j.saa.2009.09.047>.
 41. Mirle, C.R.; Raja, M.; Vasudevarao, P.; Sankararaman, S.; Kothandaraman, R. Functionalised carbazole as a cathode for high voltage non-aqueous organic redox flow batteries. *New Journal of Chemistry* **2020**, *44*, 14401–14410, <https://doi.org/10.1039/D0NJ02543G>.
 42. Uddin, S.; Hossain, Md.S.; Latif Md.A.; Karim, Md.R.; Mohapatra, R.K.; Zahan, Md.K. E. Antimicrobial activity of Mn complexes incorporating Schiff bases: A short review. *American Journal of Heterocyclic Chemistry* **2019**, *5*, 27-36. <https://doi.org/10.11648/j.ajhc.20190502.12>.
 43. Li, Y.; Jun, T.; Bo-Chu, W.; Lian-Cai, Z.H.U. Synthesis, characterization, and anticancer activity of emodin-Mn (II) metal complex. *Chinese Journal of Natural Medicines* **2014**, *12*, 937–942, [https://doi.org/10.1016/S1875-5364\(14\)60137-0](https://doi.org/10.1016/S1875-5364(14)60137-0).
 44. Irfandi, R.; Raya, I. Potential anticancer activity of Mn (II) complexes containing arginine dithiocarbamate ligand on MCF-7 breast cancer cell lines. *Annals of Medicine and Surgery* **2020**, *60*, 396–402, <https://doi.org/10.1016/j.amsu.2020.11.018>.

Supplementary materials

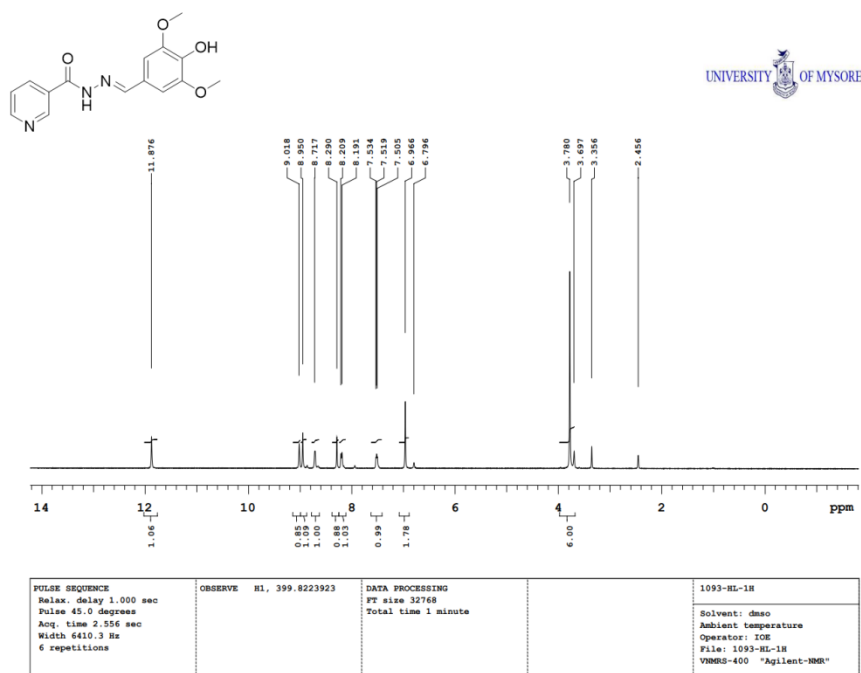


Figure S1. ¹H NMR spectrum of ligand (HL).

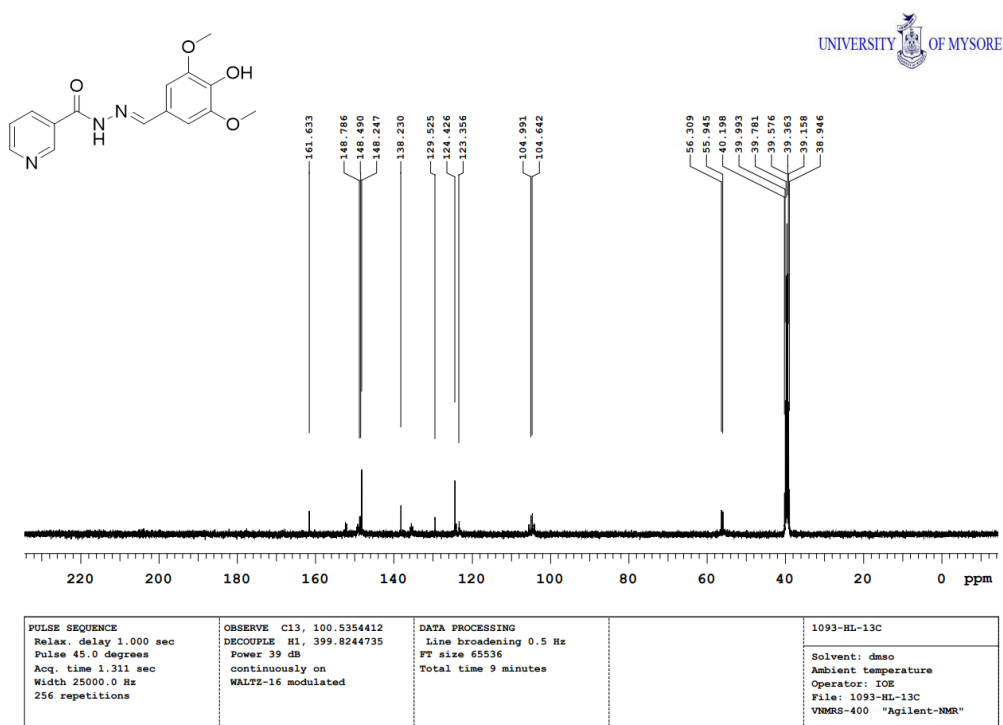


Figure S2. ¹³C-Spectrum of the ligand (HL).

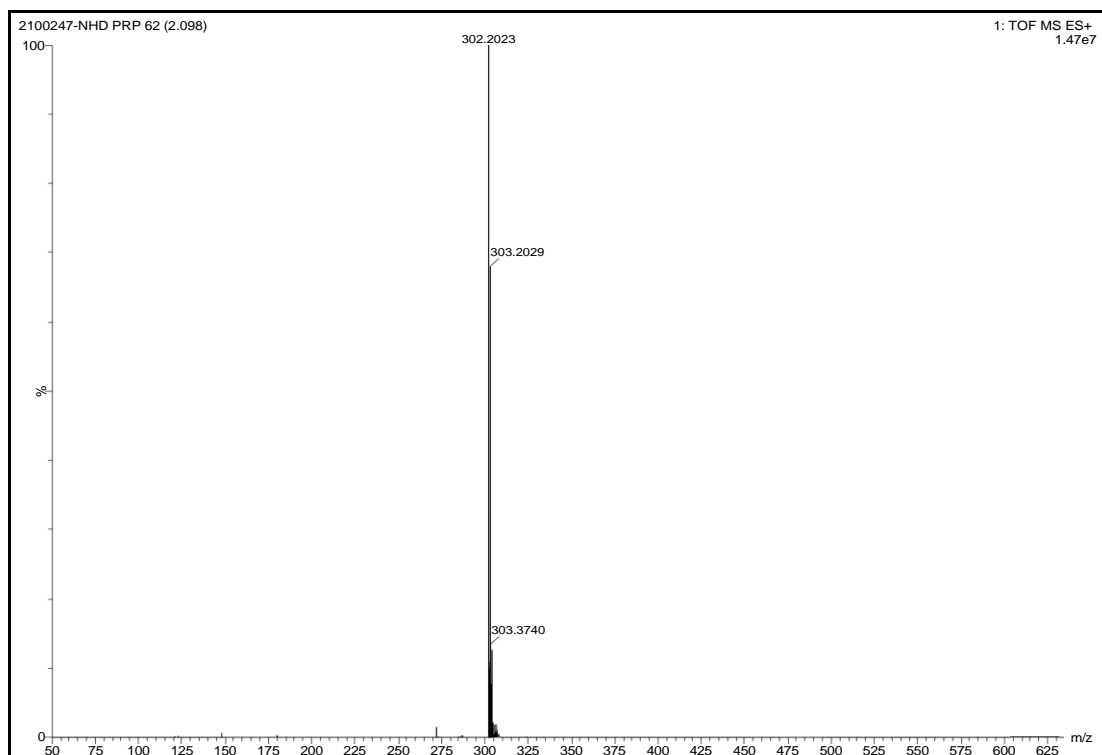


Figure S3. Mass spectrum of ligand (HL).

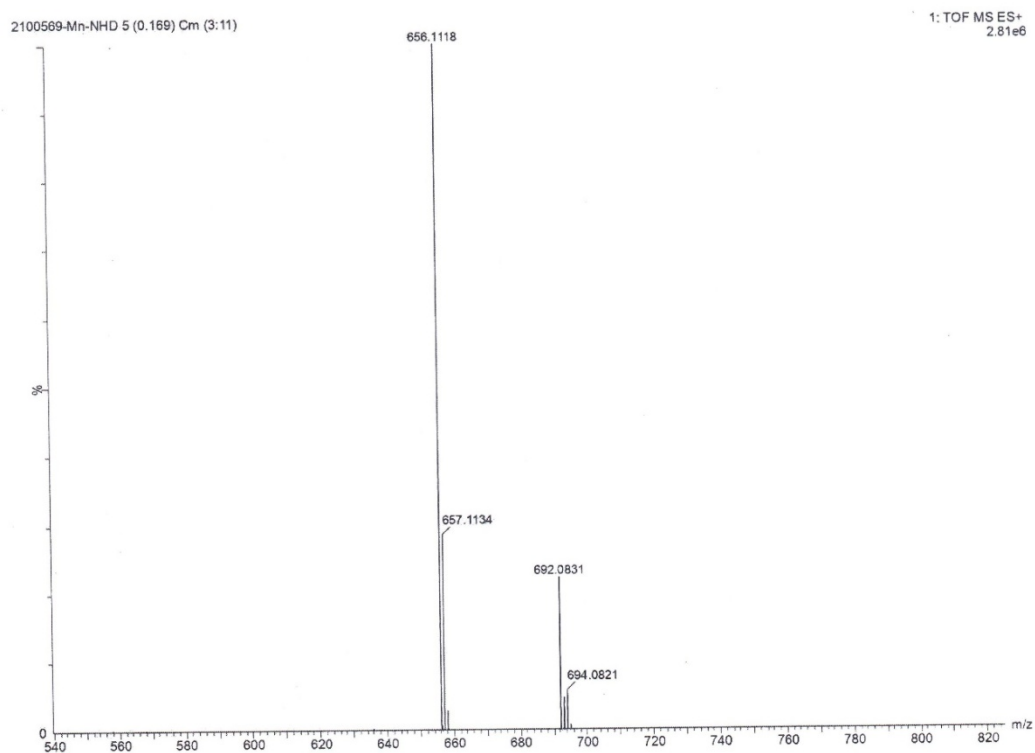


Figure S4. Mass spectrum of Mn(II) complex (1).

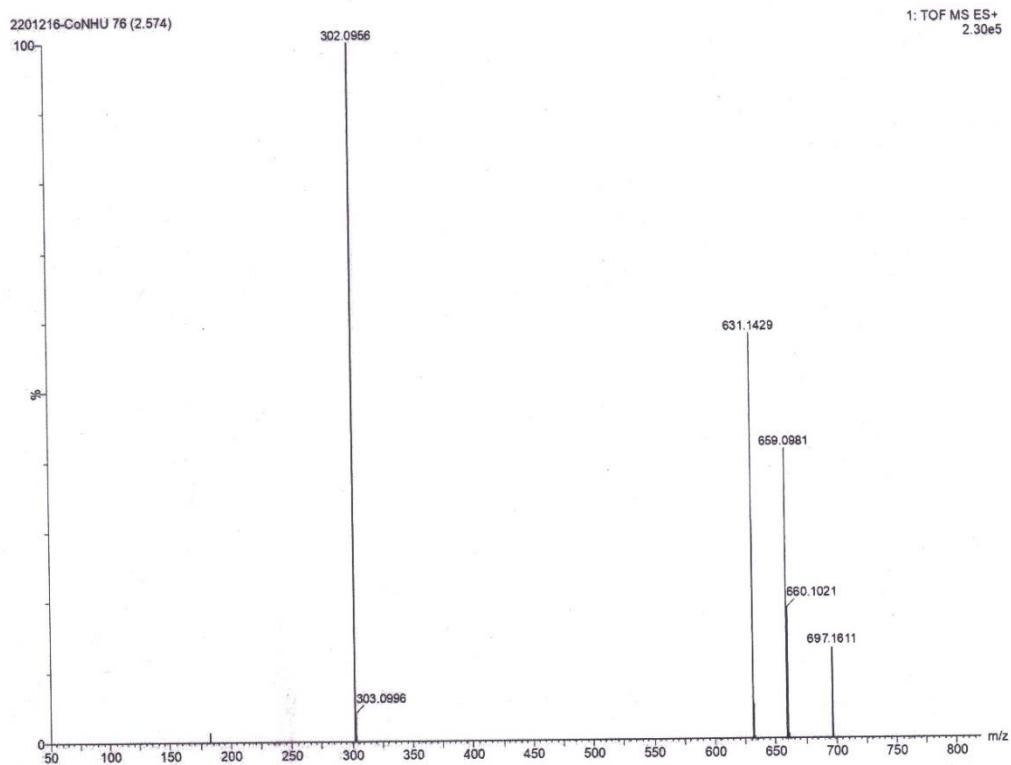


Figure S5. Mass spectrum of Co(II) complex (2).

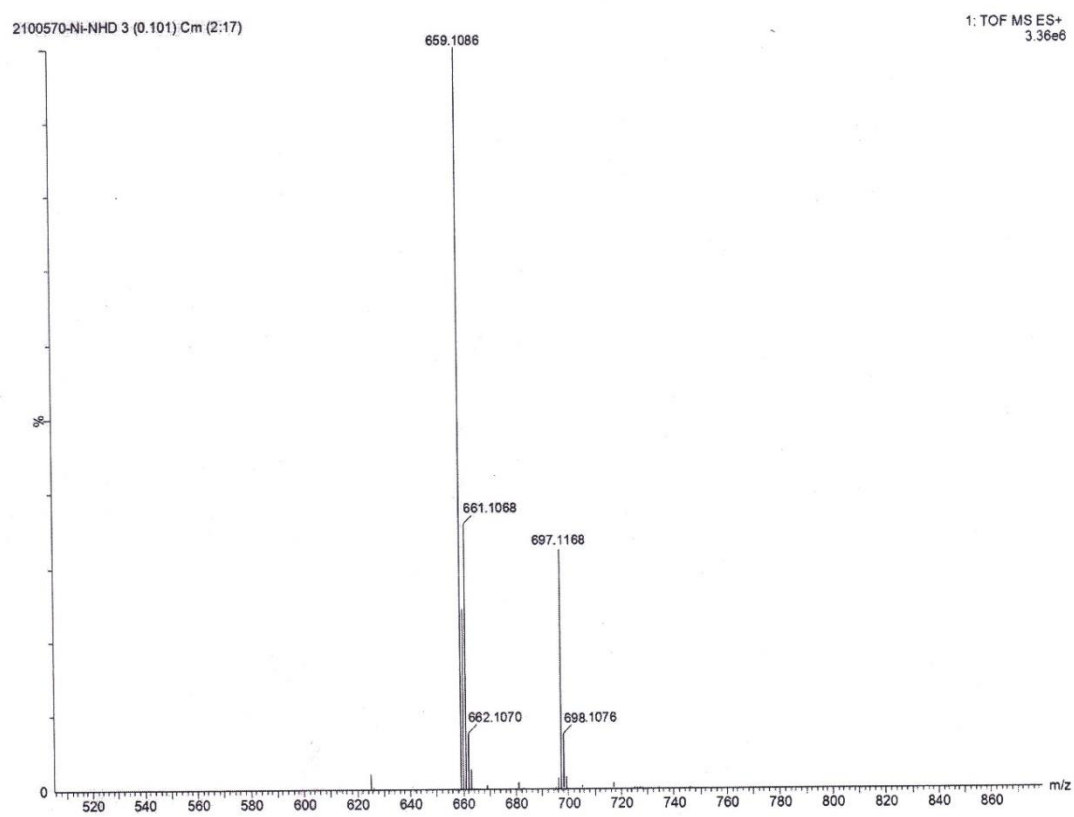


Figure S6. Mass spectrum of Ni(II) complex (3).